Results in Chemistry 27 (2026) 103398

Contents lists available at ScienceDirect

Results in Chemistry

journal homepage: www.sciencedirect.com/journal/results-in-chemistry

Synthesis, characterization and photolysis efficiency of caged nerve growth factor mimetics

Bence Szabó [a,b], Zoltán Mucsi [a,c], Attila Csomos [a,d], Ervin Kovács [a,e], Arnold Steckel [f], Gábor Turczel [g], Balázs Rózsa [a,h,i,*], Levente Cseri [a,**]

[a] BrainVisionCenter, Liliom utca 43-45, H-1094 Budapest, Hungary
[b] Department of Organic Chemistry and Technology, Budapest University of Technology and Economics, Műegyetem rakpart 3, H-1111 Budapest, Hungary
[c] Institute of Chemistry, Faculty of Materials Science and Engineering, University of Miskolc, H-3515 Miskolc, Hungary
[d] Department of Inorganic Chemistry, Institute of Chemistry, Eötvös Loránd University, Pázmány Péter sétány 1/A, H-1117 Budapest, Hungary
[e] Institute of Materials and Environmental Chemistry, HUN-REN Research Centre for Natural Sciences, Magyar tudósok körútja 2, H-1117 Budapest, Hungary
[f] MTA-ELTE Lendület (Momentum) Ion Mobility Mass Spectrometry Research Group, ELTE Eötvös Loránd University, Faculty of Science, Institute of Chemistry, Pázmány Péter sétány 1/A, H-1117 Budapest, Hungary
[g] NMR Research Laboratory, Centre for Structural Science, HUN-REN Research Centre for Natural Sciences, Magyar tudósok körútja 2, H-1117 Budapest, Hungary
[h] The Faculty of Information Technology, Pázmány Péter Catholic University, Práter utca 50, H-1083 Budapest, Hungary
[i] Laboratory of 3D Functional Network and Dendritic Imaging, HUN-REN Institute of Experimental Medicine, 43 Szigony utca, H-1083 Budapest, Hungary

ARTICLE INFO

Keywords:
Uncaging
Photolysis
Quantum yield
Photochemistry
NGF
Neurochemistry

ABSTRACT

Neurodegenerative disorders and traumatic injuries of the central nervous system constitute a major global health burden, affecting millions of individuals worldwide. Within the human body, numerous bioactive molecules are essential for neuronal development and survival, among which nerve growth factor (NGF) is one of the most critical neurotrophic proteins. Although application of the native protein has been associated with significant limitations, small-molecular NGF mimetics represent a promising alternative. A particularly attractive strategy for targeted delivery is the use of caged compounds in combination with photo-uncaging. In this work, several caged derivatives of the NGF mimetic compounds, B-355252 and LM11A-31, with coumarin and *o*-nitrobenzyl photolabile protecting groups (PPGs) were developed and characterized. The aqueous solubility of the newly synthesized molecules at physiological pH in aqueous media was determined, leading to the development of a biologically more suitable derivative. The spectroscopic properties and photo-uncaging behaviour of the molecules were also examined in both organic and aqueous media, complemented by density functional theory (DFT) calculations to investigate the uncaging mechanism. High-performance liquid chromatography (HPLC) analyses demonstrated the clean release of the bioactive compounds in aqueous media upon light irradiation of the samples at 365 nm. Finally, a method for determining uncaging quantum yields was developed, using the light-induced *E–Z* isomerisation process of dimethylazobenzene as a reference reaction.

1. Introduction

Neurodegenerative diseases and injuries to the central nervous system affect the lives of millions worldwide. The phenomena associated with these conditions, such as excessive nerve cell death or the disruption of connections between cells, can lead to the loss of certain bodily functions and a general deterioration in quality of life. In recent decades, several proteins that play a significant role in regulating nervous system processes have been identified. One of the most important families of such proteins are called neurotrophins, with the brain-derived neurotrophic factor (BDNF) and the nerve growth factor (NGF) being the most well-known among them. First isolated by Nobel laureates Rita Levi-Montalcini and Stanley Cohen in 1954 [1], NGF is involved in several crucial processes: it participates in the differentiation and maturation of nerve cells [2], has a neuroprotective effect [3], and influences the growth of developing neurites. Subsequent experiments showed that axons not only grow more intensively in the presence of the protein, but they also turn towards its concentration gradient, meaning NGF acts as a

* Corresponding author at: BrainVisionCenter, Liliom utca 43-45, H-1094 Budapest, Hungary.
** Corresponding author.
E-mail addresses: rozsabal@koki.hu (B. Rózsa), levente.cseri@brainvisioncenter.com (L. Cseri).

https://doi.org/10.1016/j.rechem.2026.103398
Received 16 April 2026; Accepted 4 May 2026
Available online 6 May 2026
2211-7156/© 2026 The Authors. Published by Elsevier B.V. This is an open access article under the CC BY license (http://creativecommons.org/licenses/by/4.0/).

chemical guidance cue for the growth cones of developing axons [4]. In line with these properties, several experiments have attempted to use the compound for therapeutic purposes, but the use of the native protein has proven to be limited in several respects [5] and has led to serious side effects, such as neuropathic pain, hypophagia and the hyperinnervation of cerebral blood vessels [6]. As a result of these experiments, researchers turned to small-molecule compounds, discovering several of them that can exert a similar effect to NGF by binding to its receptors, thus offering an alternative to the protein in possible treatments. As the base of this work, two different small-molecule compounds known in the literature as B-355252 and LM11A-31 were selected as they both have been previously demonstrated to exert similar effects to those of NGF by binding to its receptors. B-355252 has been shown to have neuroprotective effects against stroke [7], glutamate induced excitotoxicity [8], and also in a brain hypoxia model [9], while also increasing cell viability in an in vitro Parkinson's model [10]. Furthermore, the molecule was able to increase NGF induced neurite elongation even in the presence of sub-physiological concentrations of the protein [11]. LM11A-31 was also proven to have neuroprotective effects, inhibiting the neurodegenerative mechanisms and neuroinflammation associated with Alzheimer's [12,13], and preventing the breakdown of the blood-retinal barrier in mice with diabetes [14]. In addition, it was shown to stimulate neurogenesis in the hippocampus and to help restore spatial memory following traumatic brain injury [15], while also promoting neuronal recovery and neurite elongation in mice following nerve injuries [16,17]. Based on these properties, these small molecular compounds could be important tools in future therapy. However, to achieve the desired biological response without off-target effects, it is very important to control the release of these active substances in both space and time. A promising approach in medicinal chemistry to achieve this is the use of photolabile protecting groups (PPGs) [18]. These groups can be used to temporarily inactivate a substance by binding them through a covalent bond, creating a caged compound. Then, upon light irradiation of the appropriate wavelength, the covalent bond between the PPG and the protected compound can be cleaved in a process called uncaging, resulting in the release of the active substance. Such compounds are therefore well suited for use in various laser microscopy techniques, where the caged form of a bioactive compound is introduced into the system and then released with high spatiotemporal precision using a focused laser. Although the use of PPGs offers many advantages, the photochemical characterization of caged compounds can prove to be a challenge, with the uncaging quantum yield (Φ) being the most difficult property to determine. This value is defined as the probability that the absorption of a single photon will result in the photolysis of a caged molecule. Based on this definition, to quantify this value, the photolysis of the caged compounds needs to be studied as a function of the number of photons absorbed by the sample upon irradiation. While the concentration of the starting and the released compound can be easily measured, accurately measuring photon flux has been more challenging. For this purpose, actinometry is widely used. Actinometers are different photochemical reactions with known quantum yields [19]. This means that by performing and monitoring these reactions, the photon flux of the used experimental setup can be measured. However, this method can only be properly used in setups where the geometric path length of the light is known, as the absorption of the sample is necessary for calculations. Unfortunately, in the majority of photoreactors there is no well-defined geometric path length, making the use of actinometry inaccurate.

In this work, we report the synthesis and photochemical characterization of novel caged derivatives of the small-molecular NGF mimetic compounds B-355252 and LM11A-31 (Fig. 1). For the synthesis of these compounds, both coumarin and nitrobenzyl derivatives were considered as caging groups. A method, based on the work of Casimiro et al. [20], using the isomerisation of 4,4′-dimethylazobenzene as a photochemical standard was developed and applied, enabling the measurement of uncaging quantum yield in systems where the geometric path length is unknown. The photolysis of the new caged NGF mimetics was studied experimentally and with the use of density functional theory (DFT) calculations.

2. Materials and methods

2.1. Materials

For the synthesis of the compounds, commercially available chemicals and solvents were used, which were obtained from the following companies: Sigma-Aldrich (Merck), VWR, Doug Discovery (Fluorochem), Molar Chemicals. All chemicals were used as received without further purification.

2.2. Synthetic and analytical procedures

For the microwave reactions, an Anton Paar Monowave 450 type reactor was used. The reactions were monitored with TLC (thin layer chromatography) and a reversed phase (U)HPLC-UV–Vis-MS system. The TLC experiments were performed with Merck Kieselgel 60 F_{254} silica plate and were visualized under a UV lamp, in some cases using an iodine chamber or Pancaldi's solution for staining. (U)HPLC-UV–Vis-MS measurements were performed with a Nexera LC-40 (U)HPLC equipped with an SPD-M40 photodiode array detector and LCMS-2020 mass spectrometer. The used column was an Ascentis Express 90 Å C18; 50 mm × 2.1 mm; 2 μm. The crude products were purified by either normal phase flash chromatography or reversed phase preparative HPLC. In both cases, the eluent system used is indicated in the corresponding synthetic procedure. For flash chromatography, an Interchim PuriFlash XS 520 Plus system was used with different sized PuriFlash Interchim or RediSep Bronze flash columns. The preparative HPLC was carried out with a Teledyne ACCQ Prep HP150 instrument equipped with a

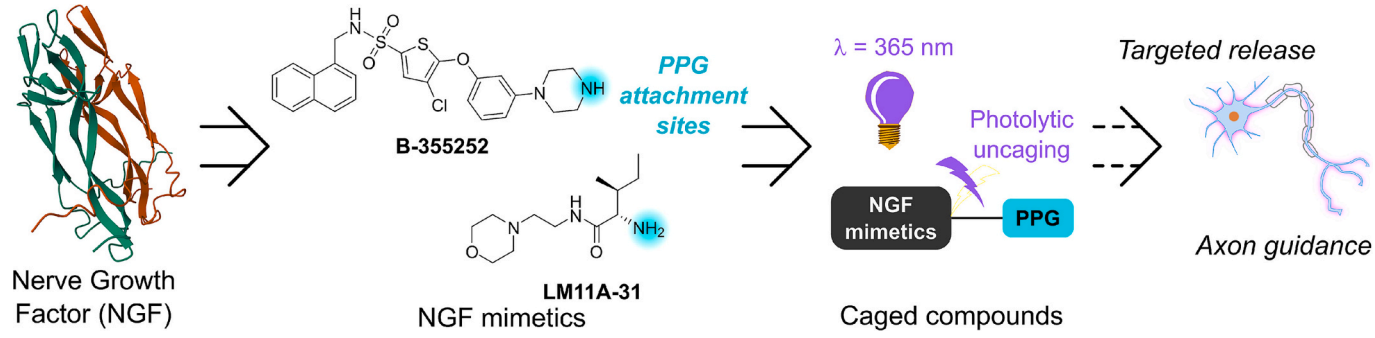

Fig. 1. Schematic overview of the research concept. Small molecular NGF mimetics are identified in the literature that contain suitable sites for photolabile protecting group (PPG) attachment. Several caged mimetics are synthesized, and the release is studied upon photo-uncaging. The new caged mimetics have potential applications in biotechnology for targeted release and axon guidance.

Phenomenex Gemini 250 × 50.0 mm; 10 μm, C18, 110 Å column. The elution flow rate was 120 mL min^{-1} in all cases. High-resolution mass spectra (HRMS) and NMR spectra were recorded to determine the structure and purity of the synthesized compounds. Accurate mass measurements were performed on a high-resolution Thermo Fisher Scientific Q-Exactive Focus hybrid quadrupole-orbitrap mass spectrometer equipped with heated electrospray ionization source. Samples were dissolved in acetonitrile-water 1:1 (*V/V*) solvent mixture containing 0.1% (*V/V*) formic acid. Flow injection analysis was performed using a 50 μL min^{-1} eluent flow. NMR spectra were obtained with a Varian Mercury Plus spectrometer or with Varian Unity INOVA spectrometers (Agilent Technologies) operating at an equivalent ^{1}H frequency of 300/400/500 MHz as noted in the peak reports. The chemical shift (δ) values are given in ppm, and the coupling constants (*J*) are given in Hz in all cases. The residual solvent peaks were used for chemical shift referencing. As some products were isolated as salts after purification, the trifluoroacetic acid amounts were determined with ^{19}F NMR, using 4-(trifluoromethyl)phenyl acetylene as a reference. The synthetic procedures and material characterizations are described in detail in Appendix A.

2.3. Spectroscopic measurements

The absorption and fluorescence spectra of the novel compounds were recorded with a Shimadzu UV-1900i UV-VIS Spectrophotometer and Shimadzu RF-6000 Spectrofluorimeter, using a Hellma Analytics quartz cuvette with 1 cm geometric path length. The scanning speed of the spectrophotometer was 648 nm min^{-1}, and the absorbance values were recorded every 2 nm. The fluorimeter was operated with a low sensitivity setting, 3 nm spectral width and 600 nm min^{-1} scanning speed, with values recorded either every 0.2 nm or 1 nm.

2.4. Photolysis experiments

The isomerisation reactions of the reference and the uncaging experiments of the caged compounds were carried out in a ThalesNano PhotoCube photoreactor. Solutions of the caged and reference compounds were placed in the same position of the reactor and the samples were irradiated at 'low' setting, with 10% intensity 365 nm (UV) light, using only one panel and 300 rpm stirring speed in all cases. The isomerisation process of the reference compound was monitored by recording the absorption spectra of the solution after certain periods of irradiation. The uncaging processes were monitored with HPLC by taking samples from the solutions after certain periods of irradiation. Function fitting was performed using OriginPro 2018 software. The experiments and conditions are described in detail in Appendix A.

2.5. Theoretical computations

Theoretical calculations were carried out by Gaussian16 software (version C.01), [21] using the standard convergence criteria given as default. Optimization and vibrational frequencies were carried out by the B3LYP method [22] using the 6-31G(d,p) basis set and the IEFPCM method ($\varepsilon = 78.3553$ for water) at ground state [23]. Thermodynamic functions were computed at 298.15 K. For wavelength prediction, the vertical excitation was modelled by the TD-B3LYP/6-31G(d,p)/[PCM (water)] level of theory using the optimized geometries. The emission wavelengths were calculated using optimized geometries provided by TD-B3LYP/6-31G(d,p)/[PCM(water)]. In the cases of S_1 state calculations, frequency computations were omitted due to the computational costs arising from the large molecular structures. The triplet state geometry was also optimized by the same level of theory (B3LYP/6-31G(d,p)/[PCM(water)]), involving the frequency calculations. Identifying the transition state (TS) geometries in the triplet state was unsuccessful with the QST3 method, due to the large molecular size. In these cases, fine relaxed scanning (0.02 Å) along the presumed reaction coordinate was used to find TS-like energy maxima, successfully confirmed by single point frequency calculations. Canonical molecular orbitals are visualized at an isovalue of 0.03.

3. Results and discussion

3.1. Design and synthesis of caged NGF mimetics

B-355252 was synthesized following procedures found in the literature [11]. As an improvement to the synthesis, 4-methoxybenzyl bromide has been successfully replaced by its much cheaper chloride analogue. Two different two-step synthetic routes were used to produce LM11A-31 (see Appendix A). PPGs with either an *o*-nitrobenzyl or coumarin scaffold were considered as these are two of the most frequently used families of photocages with straightforward synthesis and good photolytic properties [18,24]. More specifically, α-methyl-6-nitroveratryl (MeNV) and 7-diethylaminocoumarin-4-ylmethyl (DEACM) groups were selected to create the caged compounds. In the case of poor leaving groups, such as amines or alcohols, the PPGs are often linked via a carbamate or carbonate bond, ensuring that these groups can be more efficiently released during uncaging [24]. Therefore, as the chosen NGF mimetics are primary and secondary amines, their caging is preferably achieved using α-methyl-6-nitroveratryloxycarbonyl (MeNVOC) and 7- diethylaminocoumarin-4-ylmethyloxycarbonyl (DEACMOC) groups. The synthesis of the precursors of PPGs was carried out according to procedures described elsewhere [25–28] (Section 6, Appendix A). Using the different NGF mimetics and PPGs, four novel caged compounds were synthesized, in which DEACMOC was used to protect both B-355252 and LM11A-31. Additionally, B-355252 was also caged using the MeNVOC group and the DEACM group by direct *N*-alkylation (Scheme 1).

Later experiments revealed that the B-355252 derivatives have very poor solubility in aqueous media (pH = 7.4). Since these molecules are meant to be used in biological systems, it is essential that they exhibit aqueous solubility at physiological pH in the therapeutically relevant concentration range. Therefore, another caged B-355252 derivative was designed and synthesized using the 7-[bis(carboxymethyl)amino] coumarin-4-ylmethyloxycarbonyl (BCMACMOC) caging group (Scheme 2) [29], which has better water solubility due to its polar carboxyl functional groups that undergo deprotonation at physiological pH.

3.2. Solubility of the caged compounds

To evaluate the solubility of the synthesized caged compounds in aqueous media at physiological pH, saturated solutions of the compounds were prepared in pH 7.4 HEPES buffer and analysed with HPLC. As shown in Table 1, LM11A-31-DEACMOC has high water solubility, exceeding 1 mM, making it particularly suitable for biological applications. However, for the first generation of caged B-355252 derivatives, the solubility in this aqueous system could not be quantified, as it was below the limit of detection of the HPLC method used (<0.028–0.151 μM). B-355252 was shown to be effective at concentrations of 1–2 μM [11], it was essential to improve the properties of the caged compounds. The use of the BCMACMOC caging group had a beneficial effect on the solubility in the buffer, with the maximal concentration now being in the biologically relevant range. According to the calculated LOD values, this compound had at least 24–90-fold better solubility than other B-355252 derivatives. Moreover, the two carboxyl groups offer the possibility of further derivatization to further improve solubility, if the application requires.

3.3. Spectroscopic properties of the caged compounds

To investigate the spectroscopic properties of the new compounds, absorption and fluorescence spectra were recorded in solvents later used

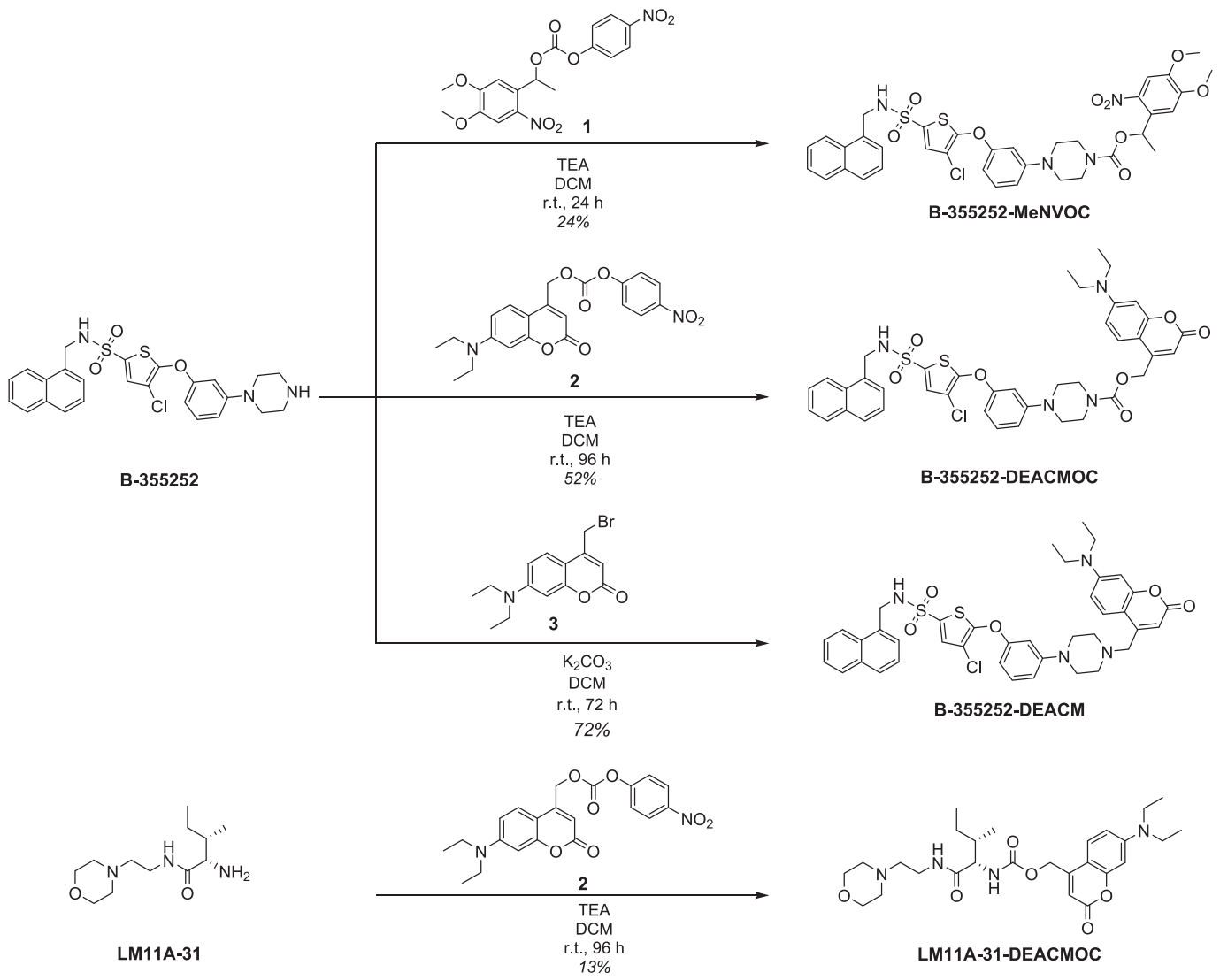

Scheme 1. Synthetic attachment of photolabile protecting groups to B-355252 and LM11A-31 to obtain caged NGF mimetics.

for the uncaging experiments. The molar absorption coefficients were determined using a dilution series of each compound. The fluorescence of the compounds was also investigated as competitive relaxation pathway to uncaging. The spectra of the different compounds are shown in Fig. 2 and the obtained values are shown in Table 2.

Based on the data in Table 2, the MeNVOC group absorbs significantly less light than the coumarin PPGs but has practically no fluorescence. It is also important to note that based on the recorded spectra, the transition necessary for uncaging can be efficiently excited with UV irradiation at the commonly available 365 nm wavelength for all compounds.

3.4. Determination of photolysis quantum yields

To evaluate the uncaging quantum yield of the new compounds, 4,4′-dimethylazobenzene (DMAB) was used as a photochemical reference. This compound undergoes a light-induced *E*–*Z* isomerisation process, which has been studied earlier in the literature and used as an actinometer by Casimiro et al. [20]. Since only the *E*-DMAB isomer is crystalline, a solution containing only this form can be prepared using the solid material. The isomerisation process can be used to obtain the quantum yield of uncaging processes according to the relationship defined by Eq. (1), if the initial absorbance, the solution volume and the experimental arrangement are identical (Section 5.1, Appendix A):

$$\frac{\left(\frac{dc}{dt}\right)_{t=0}}{\left(\frac{d[E]}{dt}\right)_{t=0}} = \frac{-\frac{\Phi_u \bullet q^* \bullet f_0^*}{V^*}}{-\frac{\Phi_{EZ} \bullet q \bullet f_0}{V}} = \frac{\Phi_u}{\Phi_{EZ}} \tag{1}$$

where c is the concentration of the caged compound, $[E]$ is the concentration of *E*-DMAB, Φ_u and Φ_{EZ} are the quantum efficiencies of the uncaging and the isomerisation processes, q^* and q are the incident photon fluxes, f^* and f are the fraction of the absorbed light (where $f = 1 - 10^{-A}$; A is the absorbance of the solution), and V and V^* are the solution volumes. Based on this equation, only the determination of the initial reaction rates is necessary to obtain the uncaging quantum yields. For the caged compounds and the reference DMAB, this was achieved by monitoring the reactions upon UV irradiation at 365 nm with spectrophotometry and HPLC, respectively. All caged compounds showed ready photolysis and release of the active compound in these experiments (Fig. 3 and Fig. S26).

Initial conversion rates were obtained by function fitting based on the kinetic equations of these processes (Fig. 4).With the obtained functions, the initial reaction rate was calculated by derivation at $t = 0$ (Sections 5.2–5.3, Appendix A). Using these values and the quantum yield of the isomerisation process of DMAB, the uncaging quantum

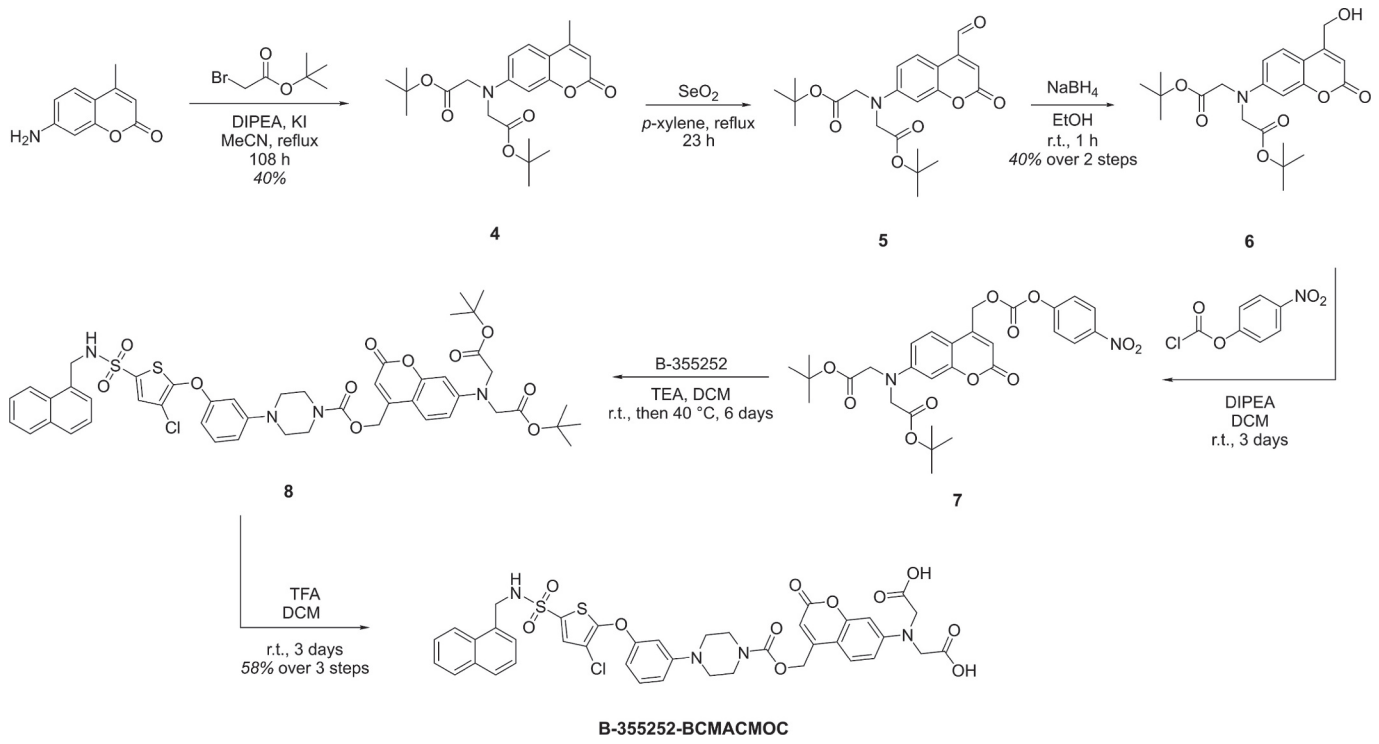

Scheme 2. Synthesis of a coumarin-caged B-355252 derivative with improved water solubility.

Table 1
Solubilities of the caged compounds in pH 7.4 aqueous buffer.

Molecule	LOD [μM]	Solubility [μM]
B-355252-MeNVOC	0.102	<LOD
B-355252-DEACMOC	0.028	<LOD
B-355252-DEACM	0.031	<LOD
LM11A-31-DEACMOC	n.d.[a]	>1000
B-355252-BCMACMOC	0.151	2.44

[a] n.d.: Not determined.

efficiencies were calculated as shown in Table 3. An important benefit of our approach is that the methodology allows for the relative determination of uncaging quantum yield in systems without a well-defined geometric path length. Nonetheless, making certain presumptions allows us to establish an idealised case where path length information is known in the form of a probability density function. With this idealised case, the photon flux can be estimated using the experimentally established initial reaction rate of DMAB isomerisation (section 5.6, Appendix A).

The first photolysis experiments with the caged compounds were carried out in MeCN, but in accordance with the biological purpose of the new compounds, tests in aqueous media were also conducted. Due to the poor solubility of certain caged B-355252 derivatives in pH 7.4 buffer, the measurements were only possible using a mixture of MeCN:HEPES-buffer 4:1. In the case of B-355252-BCMACMOC, which has

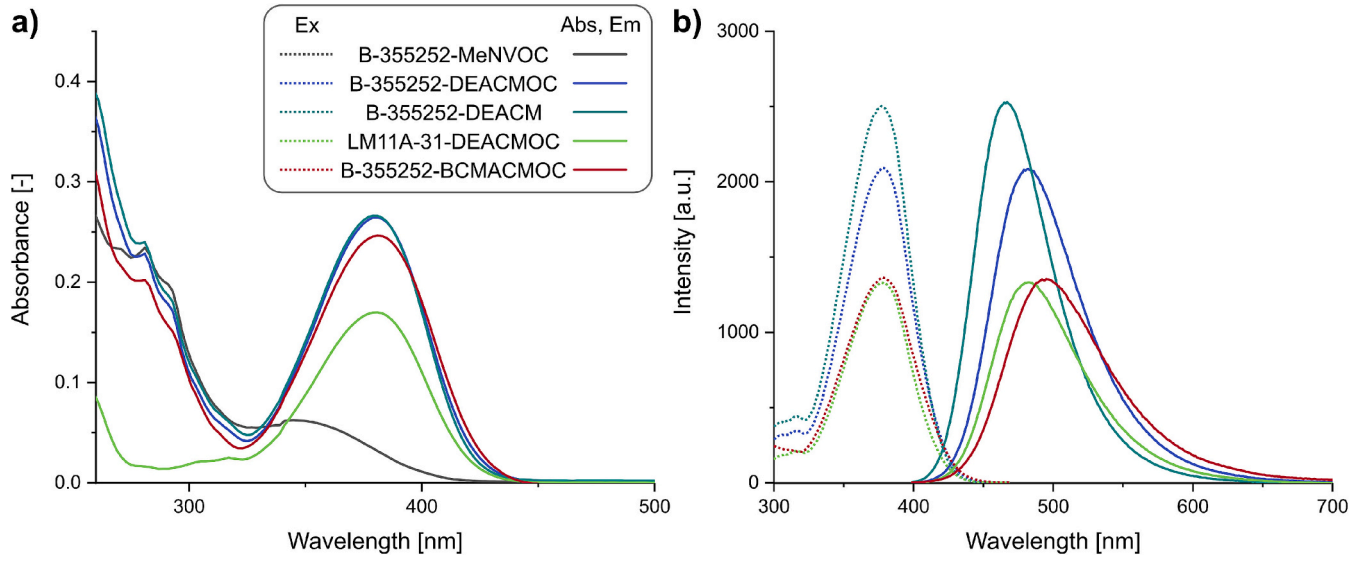

Fig. 2. (a) UV–Vis absorption spectra of caged NGF mimetics at 10 μM in MeCN:HEPES-buffer 4:1 or in MeCN:HEPES-buffer 1:4 for B-355252-BCMACMOC. (b) Fluorescence spectra of caged NGF mimetics at 2.5 μM in MeCN:HEPES-buffer 4:1 or in MeCN:HEPES-buffer 1:4 for B-355252-BCMACMOC.

Table 2
Spectroscopic properties of caged NGF mimetics in different solvents.

Molecule	ε_{365} [M^{-1} cm^{-1}]	ε_{405} [M^{-1} cm^{-1}]	λ_{max} [nm]	ε_{max} [M^{-1} cm^{-1}]	Fluorescence intensity [a.u.][a]	Stokes shift [nm]/[eV]
			MeCN			
B-355252-MeNVOC	5191	658	345	6381	n.d.[b]	–
B-355252-DEACMOC	23,014	7525	375	24,908	2567	88/0.63
B-355252-DEACM	23,933	7967	375	25,798	2518	74/0.55
LM11A-31-DEACMOC	16,124	5018	375	17,463	1413	91/0.65
B-355252-BCMACMOC	17,029	389	349	22,199	1978	88/0.73
			MeCN:HEPES 4:1			
B-355252-MeNVOC	5328	892	345	6405	n.d.[b]	–
B-355252-DEACMOC	22,355	13,492	381	26,619	834	104/0.71
B-355252-DEACM	22,984	12,917	379	26,935	1012	90/0.63
LM11A-31-DEACMOC	14,631	8397	381	17,084	532	105/0.72
B-355252-BCMACMOC	23,931	5335	365	23,931	888	103/0.78
			MeCN:HEPES 1:4			
LM11A-31-DEACMOC	10,030	13,286	391	15,526	155	110/0.71
B-355252-BCMACMOC	21,130	14,919	381	25,278	541	117/0.78
			HEPES			
LM11A-31-DEACMOC	8666	12,298	393	13,635	122	112/0.72

[a] Normalized to 1 μM.
[b] n.d.: Not detectable.

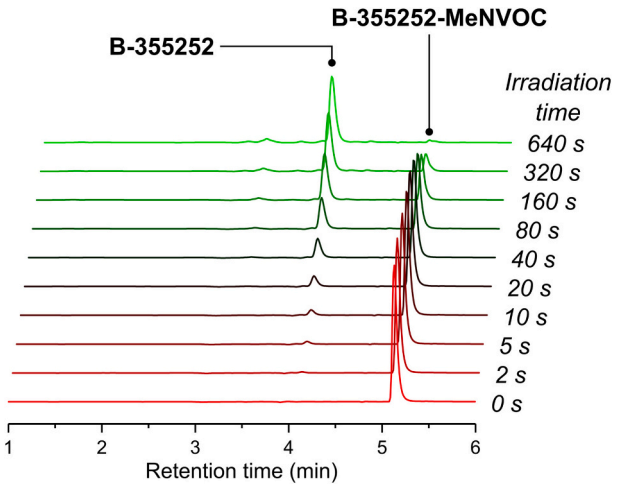

Fig. 3. HPLC chromatograms (detection at 254 nm) of B-355252-MeNVOC in MeCN:HEPES-buffer 4:1 after periods of irradiations at 365 nm in a photoreactor.

sufficient solubility for biological purposes, the addition of some MeCN was also necessary to achieve the desired absorbance, therefore it was tested using a mixture of MeCN:HEPES-buffer 1:4. As the caged LM11A-31 showed very good water solubility, it was possible to carry out the experiment using only the buffer. While the photolytic properties measured in mixed solvents may somewhat differ from those in pure buffer, the addition of acetonitrile enables the photolysis experiments at concentrations that can be reliably monitored by standard HPLC methodology with diode-array detector. The range of conducted photolysis experiments allows the direct comparison of the effects of different photocages and solvent media.

The MeNVOC caging group showed the highest quantum yield among the tested compounds both in pure MeCN and in the presence of aqueous buffer. It is also notable that the direct alkylation (B-355252-DEACM) resulted in significantly lower quantum yields than the protection through a carbamate bond (B-355252-DEACMOC). The uncaging efficiency ($\varepsilon \cdot \varphi_u$), which captures both the absorptive and photolytic properties, lies in the range of 80–500 M^{-1} cm^{-1} for all the carbamate containing photocages in aqueous media. The observed quantum yields show a monotonic change for all compounds as the aqueous content of the solvent system is increased. However, the solvent effects differ for the two NGF mimetics. For LM11A-31-DEACMOC, the φ_u increases with the water content, since the photo-generated ion pair is more stabilized in polar, protic solvents. In contrast, quantum yields exhibited a decrease for every B-355252 derivative in water-rich mixtures. This can be most likely attributed to the high hydrophobicity of B-355252, leading to the formation of nanoscopic aggregates, promoting the non-radiative quenching of the excited state and therefore hindering photolysis.

3.5. Computational studies

The photochemical reaction mechanisms of the caged compounds were investigated using density functional theory (DFT) and time-dependent DFT (TD-DFT) at the B3LYP/6-31G(d,p) level. The mechanistic pathway of the photolysis was established for B-355252-MeNVOC, B-355252-DEACM, B-355252-DEACMOC and LM11A-31-DEACMOC. The photochemical behaviour of B-355252-BCMACMOC is expected to be qualitatively similar to that of B-355252-DEACMOC.

The first step of the photolysis is the electronic excitation studied by TD-DFT. In the case of coumarin-caged molecules, the characteristic S_0–S_1 transition corresponds to the HOMO-LUMO transition of the PPG (Fig. 5). In contrast, vertical excitation to the first two excited states of B-355252-MeNVOC are forbidden (i.e. their oscillatory strength is close to 0). Here, the S_0–S_3 transition, which has relatively high oscillatory strength, corresponds to the HOMO–LUMO transition of the PPG. From the S_3 state fast relaxation is expected to the lowest excited singlet state (S_1) in accordance with Kasha's rule [30]. The forbidden nature of the S_1–S_0 is consistent with the absence of fluorescence for B-355252-MeNVOC. In all cases, subsequent intersystem crossing populates the lowest triplet state (T_1). In the triplet state (T_1), cleavage at the scissile bond proceeds via a low-barrier transition state (TS), yielding the ground-state NGF mimetic and a complementary cage fragment initially formed on the triplet surface. This bond cleavage step defines the rate-determining step of the overall photorelease pathway. Finally, the cage-derived fragment relaxes back to the electronic ground state. In the case of carbamate-linked photocages, the released carbamic acid undergoes swift decarboxylation to yield the amine form of the active NGF mimetic. The positive energy demand of the decarboxylation is countered by a strong entropic term due to the formation of carbon dioxide, that makes this step thermodynamically favoured. Overall, this mechanistic picture is consistent with general conclusions reported for related PPGs [24,31,32]. Moreover, the calculations also found an alternative cleavage pathway in T_1 for B-355252-MeNVOC. While the main photolytic pathway leads to nitrosoacetophenone, heterolytic cleavage

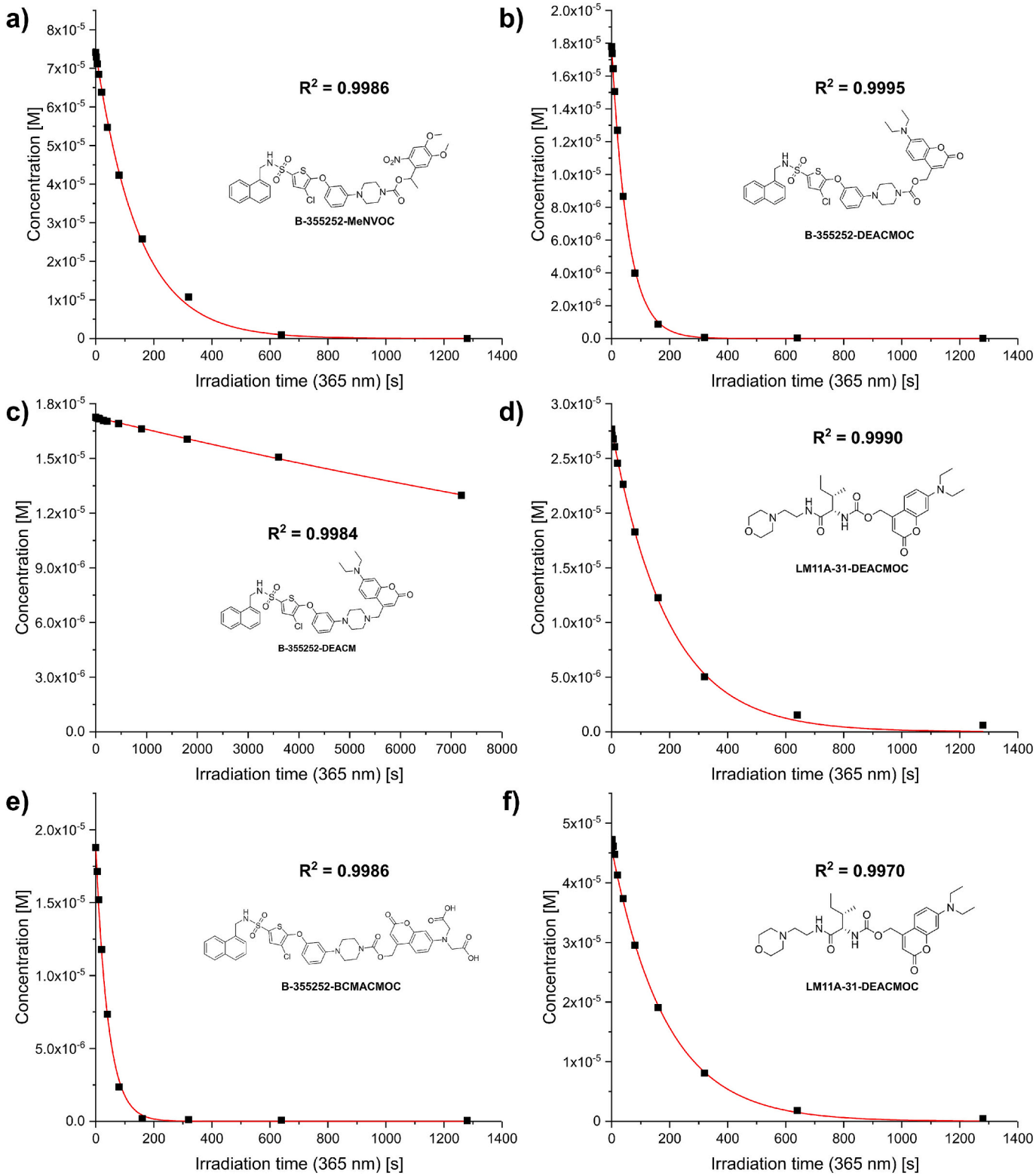

Fig. 4. Fitted functions to the data obtained during the photolysis experiments for individual compounds with a starting absorbance of 0.397 (a–d) in MeCN:HEPES buffer 4:1 mixture, (e) in MeCN:HEPES buffer 1:4 mixture and (f) in pH 7.4 HEPES buffer.

in T_1 is also possible that yields the alcohol S8 as side product (Section 8.1, Appendix A).

The mechanistic calculations revealed two important caveats to this picture in the case of B-355252-DEACM. Bond cleavage was found only to occur when the PPG-protected amino nitrogen is protonated. While protonation is thermodynamically favoured at pH 7.4 in the ground state, proton exchange with the solvent occurs in a dynamic equilibrium. Excitation of the neutral molecule or deprotonation in the excited state leads to relaxation without photolysis, which is consistent with the experimentally observed low photolysis quantum yield of B-355252-DEACM. Nevertheless, the protonated excited state showed good reactivity with the S_1 bond cleavage pathway also available.

Table 3
Calculated initial reaction rates, uncaging quantum yields and uncaging efficiency ($\varepsilon_{max}\cdot\varphi_u$) values of caged compounds using the fitted functions.

Molecule	Initial reaction rate [M s^{-1}]	φ_u [−]	$\varepsilon_{max}\cdot\varphi_u$ [M^{-1} cm^{-1}]
		MeCN	
B-355252-MeNVOC	$-3.69\cdot10^{-6}$	$1.6\cdot10^{-1}$	1033
B-355252-DEACMOC	$-7.31\cdot10^{-7}$	$3.2\cdot10^{-2}$	786
B-355252-DEACM	$-5.69\cdot10^{-9}$	$2.5\cdot10^{-4}$	6.35
LM11A-31-DEACMOC	$-1.11\cdot10^{-7}$	$4.8\cdot10^{-3}$	83.8
B-355252-BCMACMOC	$-2.04\cdot10^{-6}$	$8.8\cdot10^{-2}$	1961
		MeCN:HEPES 4:1	
B-355252-MeNVOC	$-5.01\cdot10^{-7}$	$2.2\cdot10^{-2}$	141
B-355252-DEACMOC	$-3.19\cdot10^{-7}$	$1.4\cdot10^{-2}$	369
B-355252-DEACM	$-6.78\cdot10^{-10}$	$2.9\cdot10^{-5}$	0.792
LM11A-31-DEACMOC	$-1.43\cdot10^{-7}$	$6.2\cdot10^{-3}$	106
B-355252-BCMACMOC	$-6.75\cdot10^{-7}$	$2.9\cdot10^{-2}$	700
		MeCN:HEPES 1:4	
LM11A-31-DEACMOC	$-1.82\cdot10^{-7}$	$7.9\cdot10^{-3}$	122
B-355252-BCMACMOC	$-4.44\cdot10^{-7}$	$1.9\cdot10^{-2}$	484
		HEPES	
LM11A-31-DEACMOC	$-2.44\cdot10^{-7}$	$1.0\cdot10^{-2}$	143

4. Conclusion

In this work, we have synthesized several new caged NGF mimetic compounds. For this, we used two NGF receptor agonists known in the literature as B-355252 and LM11A-31, and different photolabile caging groups, based on *o*-nitrobenzyl and coumarin moieties. Solubility experiments in pH 7.4 HEPES buffer showed that for biological purposes, only the caged LM11A-31 derivative had sufficient maximal concentration. A dicarboxylic coumarin derivative was developed to achieve enhanced aqueous solubility for a B-355252 photocage. Photolysis experiments were conducted in a photoreactor to determine the uncaging quantum yields of the different compounds under different circumstances. For this measurement, a relative technique was developed, using the initial reaction rates of the uncaging process and a reference reaction, namely the *E*–*Z* isomerisation of 4,4′-dimethylazobenzene. The experiments presented in this work demonstrate the applicability of this new method, which can be used in experimental setups where the geometric path length is not defined, along with the potential for the use of the new compounds for biological purposes. During the photolysis experiments, HPLC-MS analysis showed the steady release of the active compounds B-355252 and LM11A-31 from their photocages. Mechanistic investigations using DFT methods found photolysis pathways through triplet T_1 state.

With the aqueous solubility addressed, the photolysis experiments demonstrate the potential of the NGF mimetic photocages for targeted delivery. By delivering the caged compounds to the appropriate system, focused laser excitation, or two-photon excitation in particular, could result in the release of the active molecules with very high spatiotemporal precision, achieving local biological responses at the site of action. Due to the biological effects of the two NGF mimetics, this could grant us the opportunity to study the mechanism of neurite growth, exert neuroprotective effects, stimulate or even guide neurite outgrowth. Future experiments with the caged NGF mimetics will focus on their two-photon absorption properties as well as their application in biological systems.

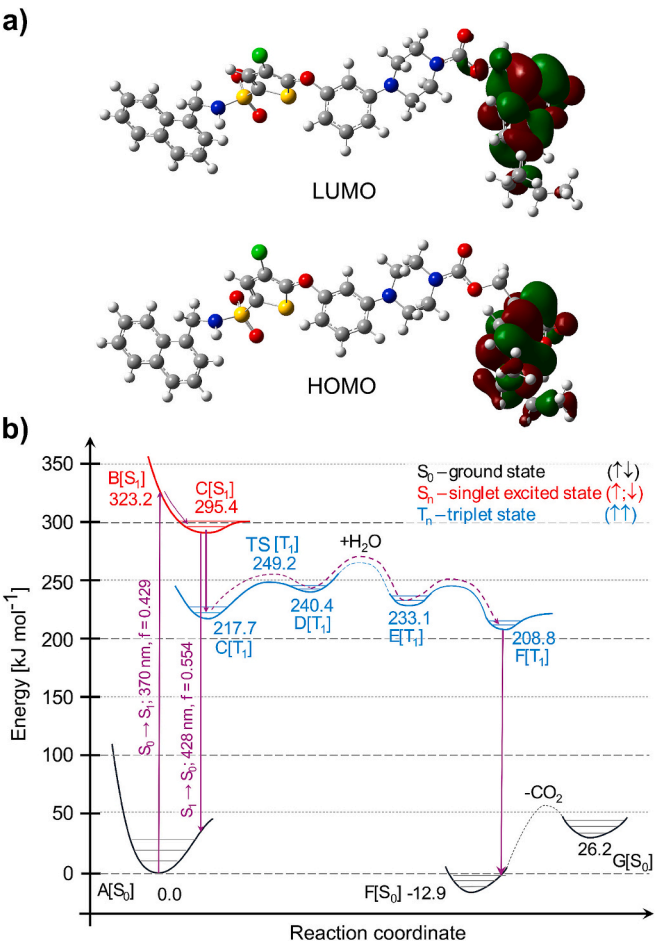

Fig. 5. (a) Visual representation of canonical HOMO and LUMO orbitals of B-355252-DEACMOC. (b) Energy level representation of the computed photolysis mechanism of compound B-355252-DEACMOC at B3LYP/6-31G(d,p)[PCM (water)] level of theory. A and G correspond to the ground state B-355252-DEACMOC and its photolysis products, including the free B-355252, respectively. Other letters denote intermediate geometries of the indicated state, as detailed in Section 8 of Appendix A. The letter *f* denotes oscillatory strength.

CRediT authorship contribution statement

Bence Szabó: Data curation, Formal analysis, Investigation, Methodology, Validation, Visualization, Writing – original draft, Writing – review & editing. **Zoltán Mucsi:** Formal analysis, Investigation, Software, Writing – original draft, Writing – review & editing. **Attila Csomos:** Data curation, Formal analysis. **Ervin Kovács:** Formal analysis, Investigation, Writing – review & editing. **Arnold Steckel:** Formal analysis, Investigation. **Gábor Turczel:** Formal analysis, Investigation. **Balázs Rózsa:** Conceptualization, Funding acquisition, Resources, Supervision. **Levente Cseri:** Conceptualization, Data curation, Formal analysis, Methodology, Project administration, Supervision, Visualization, Writing – review & editing.

Declaration of competing interest

The authors declare that they have no known competing financial interests or personal relationships that could have appeared to influence the work reported in this paper.

Acknowledgements

Projects 2025-1.3.3-NEURO-2025-00001, NKKP STARTING 152528 and EKÖP-25-4-I-ELTE-1037 have been implemented with the support

provided by the Ministry of Innovation and Technology of Hungary from the National Research, Development and Innovation Fund. This work was supported by the Bolyai János Research Scholarship of the Hungarian Academy of Sciences (BO/00365/23/7, BO/00085/24/7). B.R. is supported by GINOP-2016-00979, NKP-2017, VKE-2018-00032, GINOP-2021-00061, PM/20453-15/2020, KFI-2018-097, AMPLITUDE, GYORSÍTÓSÁV-2021-04, GINOP_PLUSZ-00143, GYORSÍTÓSÁV-2022-064, NL-2022-012, KK-2022-05, ED-2021-00190, ED-2022-00208, NKKP Excellence 153978, Demján Sándor 2024/1+1/2598. We are grateful for the possibility to use HUN-REN Cloud [33]. Z.M. was supported by the University of Miskolc within the Framework of the Institution's Scientific Excellence Support Program (ME-TKTP-2025-018).

Appendix A. Supplementary data

Supplementary data to this article can be found online at https://doi.org/10.1016/j.rechem.2026.103398.

Data availability

Data will be made available on request.

References

[1] S. Cohen, R. Levi-Montalcini, V. Hamburger, A nerve growth-stimulating factor isolated from sarcomas 37 and 180, Proc. Natl. Acad. Sci. 40 (1954) 1014–1018, https://doi.org/10.1073/pnas.40.10.1014.

[2] A. De Boer, E.M. Van Buel, G.J. Ter Horst, Love is more than just a kiss: a neurobiological perspective on love and affection, Neuroscience 201 (2012) 114–124, https://doi.org/10.1016/j.neuroscience.2011.11.017.

[3] T. Kume, H. Nishikawa, H. Tomioka, H. Katsuki, A. Akaike, S. Kaneko, T. Maeda, T. Kihara, S. Shimohama, p75-mediated neuroprotection by NGF against glutamate cytotoxicity in cortical cultures, Brain Res. 852 (2000) 279–289, https://doi.org/10.1016/S0006-8993(99)02226-X.

[4] R.W. Gundersen, J.N. Barrett, Neuronal chemotaxis: chick dorsal-root axons turn toward high concentrations of nerve growth factor, Science 206 (1979) 1079–1080, https://doi.org/10.1126/science.493992.

[5] S. Maliartchouk, Y. Feng, L. Ivanisevic, T. Debeir, A. Cuello, K. Burgess, H. Saragovi, A designed peptidomimetic agonistic ligand of TrkA nerve growth factor receptors, Mol. Pharmacol. 57 (2000) 385–391, https://doi.org/10.1016/S0026-895X(24)23211-9.

[6] A.M. Weissmiller, C. Wu, Current advances in using neurotrophic factors to treat neurodegenerative disorders, Transl. Neurodegener. 1 (2012) 14, https://doi.org/10.1186/2047-9158-1-14.

[7] H.K. Wang, J.S. Chen, C.Y. Hsu, Y.T. Su, T.C. Sung, C.L. Liang, A.L. Kwan, C.C. Wu, A novel NGF receptor agonist B355252 ameliorates neuronal loss and inflammatory responses in a rat model of cerebral ischemia, J. Inflamm. Res. 14 (2021) 2363–2376, https://doi.org/10.2147/JIR.S303833.

[8] N.S. Gliyazova, E.Y. Huh, G.C. Ibeanu, A novel phenoxy thiophene sulphonamide molecule protects against glutamate evoked oxidative injury in a neuronal cell model, BMC Neurosci. 14 (2013) 93, https://doi.org/10.1186/1471-2202-14-93.

[9] U. Chimeh, M.A. Zimmerman, N. Gilyazova, P.A. Li, B355252, a novel small molecule, confers neuroprotection against cobalt chloride toxicity in mouse hippocampal cells through altering mitochondrial dynamics and limiting autophagy induction, Int. J. Med. Sci. 15 (2018) 1384–1396, https://doi.org/10.7150/ijms.24702.

[10] N.S. Gliyazova, G.C. Ibeanu, The chemical molecule B355252 is neuroprotective in an in vitro model of Parkinson's disease, Cell. Mol. Neurobiol. 36 (2016) 1109–1122, https://doi.org/10.1007/s10571-015-0304-5.

[11] A.L. Williams, S.R. Dandepally, N. Gilyazova, S.M. Witherspoon, G. Ibeanu, Microwave-assisted synthesis of 4-chloro-N-(naphthalen-1-ylmethyl)-5-(3-(piperazin-1-yl)phenoxy)thiophene-2-sulfonamide (B-355252): a new potentiator of nerve growth factor (NGF)-induced neurite outgrowth, Tetrahedron 66 (2010) 9577–9581, https://doi.org/10.1016/j.tet.2010.09.028.

[12] T.V.V. Nguyen, L. Shen, L. Vander Griend, L.N. Quach, N.P. Belichenko, N. Saw, T. Yang, M. Shamloo, T. Wyss-Coray, S.M. Massa, F.M. Longo, Small molecule p75NTR ligands reduce pathological phosphorylation and misfolding of tau, inflammatory changes, cholinergic degeneration, and cognitive deficits in AβPPL/S transgenic mice, J. Alzheimer's Dis 42 (2014) 459–483, https://doi.org/10.3233/JAD-140036.

[13] M.L. James, N.P. Belichenko, A.J. Shuhendler, A. Hoehne, L.E. Andrews, C. Condon, T.V.V. Nguyen, V. Reiser, P. Jones, W. Trigg, J. Rao, S.S. Gambhir, F. M. Longo, [18F]GE-180 PET detects reduced microglia activation after LM11A-31 therapy in a mouse model of Alzheimer's disease, Theranostics 7 (2017) 1422–1436, https://doi.org/10.7150/thno.17666.

[14] S.L. Elshaer, A. Alwhaibi, R. Mohamed, T. Lemtalsi, M. Coucha, F.M. Longo, A. B. El-Remessy, Modulation of the p75 neurotrophin receptor using LM11A-31 prevents diabetes-induced retinal vascular permeability in mice via inhibition of inflammation and the RhoA kinase pathway, Diabetologia 62 (2019) 1488–1500, https://doi.org/10.1007/s00125-019-4885-2.

[15] J. Shi, F.M. Longo, S.M. Massa, A small molecule p75NTR ligand protects neurogenesis after traumatic brain injury, Stem Cells 31 (2013) 2561–2574, https://doi.org/10.1002/stem.1516.

[16] C. Tep, T.H. Lim, P.O. Ko, S. Getahun, J.C. Ryu, V.M. Goettl, S.M. Massa, M. Basso, F.M. Longo, S.O. Yoon, Oral administration of a small molecule targeted to block proNGF binding to p75 promotes myelin sparing and functional recovery after spinal cord injury, J. Neurosci. 33 (2013) 397–410, https://doi.org/10.1523/JNEUROSCI.0399-12.2013.

[17] G.N. Yin, J. Ock, A. Limanjaya, N.N. Minh, S.S. Hong, T. Yang, F.M. Longo, J. K. Ryu, J.K. Suh, Oral administration of the p75 neurotrophin receptor modulator, LM11A-31, improves erectile function in a mouse model of cavernous nerve injury, J. Sex. Med. 18 (2021) 17–28, https://doi.org/10.1016/j.jsxm.2020.10.015.

[18] C. Bao, L. Zhu, Q. Lin, H. Tian, Building biomedical materials using photochemical bond cleavage, Adv. Mater. 27 (2015) 1647–1662, https://doi.org/10.1002/adma.201403783.

[19] J. Rabani, H. Mamane, D. Pousty, J.R. Bolton, Practical chemical actinometry—a review, Photochem. Photobiol. 97 (2021) 873–902, https://doi.org/10.1111/php.13429.

[20] L. Casimiro, L. Andreoni, J. Groppi, A. Credi, R. Métivier, S. Silvi, 4,4′-Dimethylazobenzene as a chemical actinometer, Photochem. Photobiol. Sci. 21 (2022) 825–833, https://doi.org/10.1007/s43630-021-00162-3.

[21] M.J. Frisch, G.W. Trucks, H.B. Schlegel, G.E. Scuseria, M.A. Robb, J.R. Cheeseman, G. Scalmani, V. Barone, B. Mennucci, G.A. Petersson, H. Nakatsuji, M. Caricato, X. Li, H.P. Hratchian, A.F. Izmaylov, J. Bloino, G. Zheng, J.L. Sonnenberg, M. Hada, M. Ehara, K. Toyota, R. Fukuda, J. Hasegawa, M. Ishida, T. Nakajima, Y. Honda, O. Kitao, H. Nakai, T. Vreven, J.A. Montgomery Jr., J.E. Peralta, F. Ogliaro, M. Bearpark, J.J. Heyd, E. Brothers, K.N. Kudin, V.N. Staroverov, R. Kobayashi, J. Normand, K. Raghavachari, A. Rendell, J.C. Burant, S.S. Iyengar, J. Tomasi, M. Cossi, N. Rega, J.M. Millam, M. Klene, J.E. Knox, J.B. Cross, V. Bakken, C. Adamo, J. Jaramillo, R. Gomperts, R.E. Stratmann, O. Yazyev, A.J. Austin, R. Cammi, C. Pomelli, J.W. Ochterski, R.L. Martin, K. Morokuma, V.G. Zakrzewski, G.A. Voth, P. Salvador, J.J. Dannenberg, S. Dapprich, A.D. Daniels, Ö. Farkas, J.B. Foresman, J. V Ortiz, J. Cioslowski, D.J. Fox, Gaussian 16, Revision C.01, Gaussian Inc Wallingford CT. (2016).

[22] A.D. Becke, Density-functional thermochemistry. III. The role of exact exchange, J. Chem. Phys. 98 (1993) 5648–5652, https://doi.org/10.1063/1.464913.

[23] J. Tomasi, B. Mennucci, R. Cammi, Quantum mechanical continuum solvation models, Chem. Rev. 105 (2005) 2999–3094, https://doi.org/10.1021/cr9904009.

[24] P. Klán, T. Šolomek, C.G. Bochet, A. Blanc, R. Givens, M. Rubina, V. Popik, A. Kostikov, J. Wirz, Photoremovable protecting groups in chemistry and biology: reaction mechanisms and efficacy, Chem. Rev. 113 (2013) 119–191, https://doi.org/10.1021/cr300177k.

[25] C. Gao, Z.L. Luan, Q. Zhang, S. Yang, S.J. Rao, D.H. Qu, H. Tian, Triggering a [2] rotaxane molecular shuttle by a photochemical bond-cleavage strategy, Org. Lett. 19 (2017) 1618–1621, https://doi.org/10.1021/acs.orglett.7b00393.

[26] T.H. Koch, B.L. Barthel, H.H. Yin, R. Tamura, A. Balabanova, Anthracycline Prodrugs and Methods of Making and Using the Same, WO2016176332, 2016.

[27] G. Bassolino, C. Nançoz, Z. Thiel, E. Bois, E. Vauthey, P. Rivera-Fuentes, Photolabile coumarins with improved efficiency through azetidinyl substitution, Chem. Sci. 9 (2018) 387–391, https://doi.org/10.1039/c7sc03627b.

[28] Z. Gao, P. Yuan, D. Wang, Z. Xu, Z. Li, X. Shao, Photo-controlled release of fipronil from a coumarin triggered precursor, Bioorg. Med. Chem. Lett. 27 (2017) 2528–2535, https://doi.org/10.1016/j.bmcl.2017.03.091.

[29] B. Briand, N. Kotzur, V. Hagen, M. Beyermann, A new photolabile carboxyl protecting group for native chemical ligation, Tetrahedron Lett. 49 (2008) 85–87, https://doi.org/10.1016/j.tetlet.2007.11.028.

[30] M. Kasha, Characterization of electronic transitions in complex molecules, Discuss. Faraday Soc. 9 (1950) 14–19, https://doi.org/10.1039/DF9500900014.

[31] A. Romano, I. Roppolo, M. Giebler, K. Dietliker, Možina, P. Šket, I. Mühlbacher, S. Schlögl, M. Sangermano, Stimuli-responsive thiol-epoxy networks with photo-switchable bulk and surface properties, RSC Adv. 8 (2018) 41904–41914, https://doi.org/10.1039/c8ra08937j.

[32] R. Schmidt, D. Geissler, V. Hagen, J. Bendig, Mechanism of photocleavage of (coumarin-4-yl)methyl esters, J. Phys. Chem. A 111 (2007) 5768–5774, https://doi.org/10.1021/jp071521c.

[33] M. Héder, E. Rigó, D. Medgyesi, R. Lovas, S. Tenczer, F. Török, A. Farkas, M. Emődi, J. Kadlecsik, G. Mező, Á. Pintér, P. Kacsuk, The past, present and future of the ELKH Cloud, Inform. Tarsad. 22 (2022) 128, https://doi.org/10.22503/inftars.xxii.2022.2.8.